HAL
open science

Grafting of a new bis-silylamido aluminum species on silica: insight from solid-state NMR into interactions with the surface

Tom Vancompernolle, Nicolas Merle, Frédéric Capet, Iker Del rosal, Laurent Maron, Laurent Delevoye, Frédérique Pourpoint, Régis M. Gauvin

To cite this version:

Tom Vancompernolle, Nicolas Merle, Frédéric Capet, Iker Del rosal, Laurent Maron, et al.. Grafting of a new bis-silylamido aluminum species on silica: insight from solid-state NMR into interactions with the surface. Dalton Transactions, 2019, 48 (16), pp.5243 - 5252. 10.1039/c9dt00845d . hal-03096927

HAL Id: hal-03096927

https://hal.science/hal-03096927v1

Submitted on 5 Jan 2021

HAL is a multi-disciplinary open access archive for the deposit and dissemination of scientific research documents, whether they are published or not. The documents may come from teaching and research institutions in France or abroad, or from public or private research centers.

L'archive ouverte pluridisciplinaire **HAL**, est destinée au dépôt et à la diffusion de documents scientifiques de niveau recherche, publiés ou non, émanant des établissements d'enseignement et de recherche français ou étrangers, des laboratoires publics ou privés.

Please do not adjust margins

Journal Name

ARTICLE

Grafting of a new bis-silylamido aluminum species on silica: insight from ^{27}Al MAS NMR into interactions with the surface.

Received 00th January 20xx,
Accepted 00th January 20xx

DOI: 10.1039/x0xx00000x

www.rsc.org/

Tom Vancompernolle, [a] Nicolas Merle, [a] Frédéric Capet,[a] Iker Del Rosal,[b] Laurent Maron,[b] Laurent Delevoye, [a] Frédérique Pourpoint [a] and Régis M. Gauvin [a]*

The new bisamido aluminum species [AlCl{N(SiMe$_3$)$_2$}$_2$(THF)] (**1**) was prepared and fully characterized, including by ^{27}Al and ^{35}Cl solid state NMR, along with X-ray diffraction studies. **1** was grafted on silica dehydroxylated at 700 °C, affording silica-supported Al species. The resulting material (**2**) was characterized by IR, elemental analysis and ^{1}H, ^{13}C and ^{27}Al solid state MAS NMR. The 1D and 2D ^{27}Al MAS NMR studies showed the occurrence of two types of species, where the Al center adopts a tetracoordinated coordination sphere, with as additional coordinated Lewis base, either a THF ligand or a silica-surface siloxane moiety. DFT calculations allowed understanding the grafting mechanism and the spectroscopic properties of the material.

Introduction

Transition- and main group-metal amide derivatives hold a prominent position in organometallic synthesis and catalysis.[1] They are widely used either as precursors in multistep synthesis, or as entry into a given catalytic cycle, which occurs most of the time through protonolysis reactions. When considering the peculiar case of silylamides, from a practical point of view, their stability, lipophilicity and unique signature in ^{1}H and ^{13}C NMR make them convenient ligands for organometallic chemistry. Furthermore, as shown mostly by Anwander and coworker, silylamides are highly versatile precursors for the preparation of hybrid materials via grafting onto dehydroxylated silica-type supports.[2] Such reactions result in grafting of metal centres along with capping of silanols functions, thus affording surfaces devoid of protic SiOH sites.

This surface organometallic chemistry approach for the preparation of supported metallic species is highly convenient, as it may afford a precise control over the grafted species coordination sphere.[3] However, one of the questions in this field lies in the interaction between a metal center and the surface itself. This includes the assessment of the first coordination sphere, where several techniques may allow determining the number of grafted SiOM anchors, and thus most of the nature and stoichiometry of the metal ligand sets. In a second step, the study of the interaction with siloxane moieties is challenging. EXAFS, for instance, can provide such an information, though one needs input from a given model to be able to provide an overall averaged value for the atoms in the first coordination sphere of a given element. On the other hand, solid state NMR, which gives information on the molecular level is the most attractive local technique, provided that the considered nucleus is receptive and features suitable NMR properties.[4] We have for instance relied on ^{17}O surface-enriched SiO_2 to reveal interactions between siloxane groups and the metal centre in several catalytic materials.[5] A complementary approach is to rely on NMR observation of the metal center itself, where NMR parameters could indicate the nature of the bound elements. In this context, aluminum is a very suitable candidate for such a study, as it features a single sensitive isotope, ^{27}Al (S= 5/2), which is highly responsive, and for which NMR parameters such as the chemical shift or the quadrupolar coupling constant are highly dependent on the nature and geometry of the coordination sphere.

The first aluminum silylamide derivative, [Al{N(SiMe$_3$)$_2$}$_3$], was prepared in 1963, and was structurally characterized in 1969.[6] Since then, aluminum silylamides developed into a rich field of coordination and organometallic chemistry.[7] Mixed chlorosilylamide derivatives, for instance, can been prepared by adjusting reaction conditions, either as donor ligand-free or as adducts of N- or O-donors.[8] Trisamide aluminum species have been immobilized on siliceous materials by Anwander, who also developed ligand exchange resulting in catalytically more efficient species.[9] However, it seems of interest to develop a mixed surface platform such as [(≡SiO)AlCl(NR$_2$)], which could react with protic reagents (HX) into [(≡SiO)AlCl(X)] surface species, where the presence of the chloride on the aluminum center modulate electrophilicity compared to that of [(≡SiO)Al(X)$_2$] derived from [(≡SiO)Al(NR$_2$)$_2$]. In this view, we present here the synthesis and characterization of a new bisamide chloro aluminum derivative, and its grafting on dehydroxylated silica, along with detailed characterization of the resulting aluminum-grafted material.

[a.] Univ. Lille, CNRS, Centrale Lille, ENSCL, Univ. Artois, UMR 8181 - UCCS - Unité de Catalyse et Chimie du Solide, F-59000 Lille, France.
[b.] Laboratoire de Physico-Chimie des Nano-Objets, CNRS UMR 5215, Université de Toulouse, INSA, UPS, 135 avenue de Rangueil, F-31077 Toulouse, France.

Electronic Supplementary Information (ESI) available: CCDC 1884192, file with coordinates from DFT calculations. See DOI: 10.1039/x0xx00000x

Please do not adjust margins

Please do not adjust margins

Results and discussion

Complex [AlCl{N(SiMe$_3$)$_2$}$_2$(THF)] (**1**) was obtained by reacting AlCl$_3$ with 2 equivalents of Li[N(SiMe$_3$)$_2$](THF)$_x$ in toluene. After filtration to remove LiCl, crystallization from pentane at -20 °C afforded the new complex in 80 % yield as colorless crystals. Interestingly, even in the presence of excess lithium amide, no further chloride substitution occurred, in contrast with observation made by Paciorek using benzene as a solvent.[8] These authors also reported that the parent [AlCl{N(SiMe$_3$)$_2$}$_2$] species does not form adducts in the presence of NEt$_3$, most probably due to steric constraints from the bulky bistrimethylsylilamido groups. This steric protection results in [AlCl{N(SiMe$_3$)$_2$}$_2$] being present as a mononuclear species in the solid state, as shown by X-ray diffraction studies.[8]

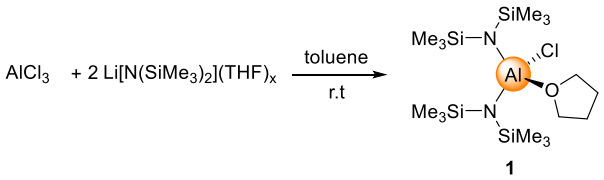

Scheme 1. Synthesis of **1**

In C$_6$D$_6$ solution, the ^{1}H NMR spectrum of **1** features 3 signals accounting for SiMe$_3$ (0.4 ppm) and for a bound THF molecule (2 multiplets at 1.1 and 4.0 ppm for β- and α- CH$_2$ protons, respectively). Integration of the SiMe and THF protons signals confirms the structure of **1**, as a THF mono-adduct. The ^{13}C NMR spectrum is also in line with the proposed structure, displaying 3 signals at 6.2 ppm (SiMe$_3$), 24.8 (β-CH$_2$ from THF) and 74.0 ppm (α-CH$_2$ from THF). The solid-state structure of **1** was determined by single crystal X-ray diffraction studies and is presented in Figure 1, along with selected bond distances and angles. The aluminum center features a distorted tetrahedral geometry, with two planar amido ligands as evidenced by the sum of angles around the N atoms (respective sums of angles for N1 and N2: 360.0 (15) and 357.90 (16)). These two planes from each amide ligand are oriented in roughly perpendicular fashion, in order to minimize steric interactions from eclipsed positions. The chloride ligand is in terminal configuration. This structure is similar to that of the scandium derivative [Sc{N(SiMe$_3$)$_2$}$_2$(Cl)THF)] recently reported by the Hayes group.[10]

Further characterization of this complex was performed using ^{27}Al and ^{35}Cl solid state NMR. Figure 2 presents the ^{27}Al QCPMG NMR spectrum. The significant second order quadrupolar coupling for the Al center induces a broadening of the signal such that acquisition had to be performed under static conditions, even at high magnetic field (18.8 T), and using a QCPMG pulse sequence to achieve high signal-to-noise ratio.[11]

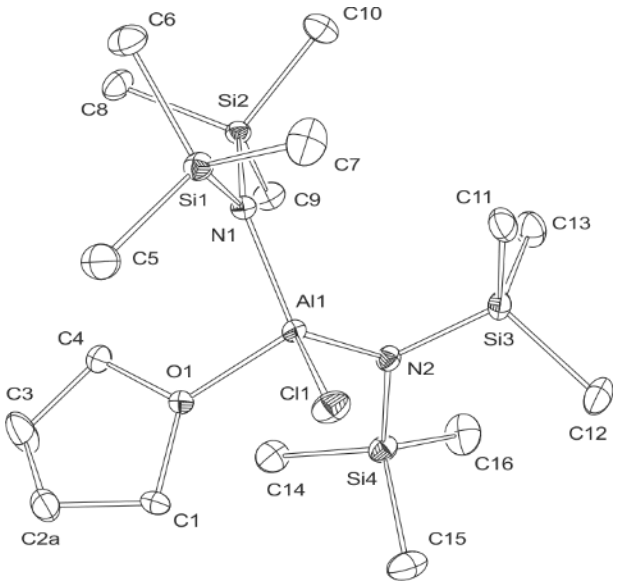

Figure 1. Solid-state structure of **1** (H atoms are omitted for the sake of clarity). Selected bond lengths (Å) and angles (°): Al(1)-Cl(1): 2.185 (1), Al(1)-N(1) : 1.833 (1), Al(1)-N(2) : 1.822 (1), Al(1)-O(1) : 1.901 (1), N(1)-Al(1)-Cl(1): 112.98 (3), N(1)-Al(1)-N(2): 123.58 (5), N(2)-Al(1)-Cl(1): 107.41 (3), O(1)-Al(1)-Cl(1): 97.81 (3), N(2)-Al(1)-O(1): 110.62 (4)

From this data, isotropic and anisotropic NMR parameters were extracted using best-fit simulations: The ^{27}Al isotropic chemical shift (δ_{iso}) is of 95 ppm, the quadrupolar coupling constant (C_Q) is of 20.4 MHz and the asymmetry parameter (η_Q) is 0.67. The quality of the fit was improved by also considering chemical shift anisotropy (δ_{CSA}= -50 ppm and η_{CSA}=0.9). The chemical shift value is in the upper range for an aluminium site in a tetrahedral configuration, while the large value of quadrupolar coupling constant is indicative of the electrical field gradient being affected by the dissymmetry within the aluminium coordination sphere, which features three different types of ligands (amide, chloride and ether), and is non-symmetrical as shown by the X-ray diffraction study (Figure 1). In addition, we were able to record the ^{35}Cl NMR spectrum of **1**, using the WURST-QCPMG sequence which enables recording ultra-wide signals such as those typically encountered with this S=7/2 nucleus (Figure 3).[12] Indeed, this nucleus was shown to be a convenient spectroscopic probe for studying organometallic and coordination compounds.[13] The best-fit simulation corresponds to a δ_{iso} value of 90 ppm and a C_Q value of 21.0 MHz (Table 1). Even though these high values of quadrupolar coupling constant are consistent with previous studies,[11,13] DFT calculations were performed to strengthen our assessment of the quadrupolar nuclei NMR parameters values. First of all, the ^{35}Cl and ^{27}Al chemical shift values of **1** were used to calibrate calculations. DFT calculations of anisotropic ^{27}Al and ^{35}Cl NMR parameters for **1** are displayed in Table 1, and are fully in line with the experimental results. Those results validate the calculation method for that kind of compounds and the structure found by X-ray diffraction.

This journal is © The Royal Society of Chemistry 20xx

Please do not adjust margins

Please do not adjust margins

Table 1. Experimental and calculated ^{27}Al and ^{35}Cl NMR parameters.

	^{27}Al			^{35}Cl		
	δ_{iso} (ppm)	C_Q (MHz)	η_Q	δ_{iso} (ppm)	C_Q (MHz)	η_Q
1	95	20.5	0.67	90	21.0	0.1
1$_{calc}$	95	20.7	0.92	90	21.7	0.14
2	95-40	-	-	na	na	na
2$_{calc}$**-a**	75	21.1	0.69	-	-	-
[(≡SiO)AlCl{N(SiMe$_3$)$_2$}(THF)] models						
2$_{calc}$**-b**	85.0	16.5	0.88	42.4	23.3	0.09
2'$_{calc}$**-b**	85.7	18.9	0.82	38.8	23.0	0.09
[(≡SiO)AlCl{N(SiMe$_3$)$_2$}] models						
2$_{calc}$**-c**	112.7	36.7	0.47	61.7	26.1	0.33
2'$_{calc}$**-c**	112.7	37.0	0.44	59.1	26.3	0.36
[(≡SiO)AlCl{N(SiMe$_3$)$_2$}(≡SiOSi≡)] models						
2$_{calc}$**-d**	88.9	25.9	0.92	54.3	24.8	0.16
2'$_{calc}$**-d**	94.3	24.4	0.71	52.7	25.1	0.14
2'$_{calc}$**-e**	90.9	25.1	0.73	90.7	25.7	0.17
2'$_{calc}$**-f**	87.2	20.7	0.97	87.9	23.9	0.16

In a further step, we probed the surface chemistry of **1** on partially dehydroxylated silica. The reactivity of **1** towards SiO_2 surface is expected to be very similar to that of the related trivalent rare-earth metal amides [Ln{N(SiMe$_3$)$_2$}$_3$],[2,14,15] namely cleavage of M-N bonds and formation of M-O bonds, release of hexamethyldisilazane (HMDS) and silylation of silanols. More precisely, it has been shown that well-defined mono-grafted rare-earth metal species can be obtained when using silica treated at 700 °C under high vacuum (10^{-5} mbar),[15] a support which bears non-interacting silanol groups as sole type of SiOH. This is evidenced by the IR spectrum comprising a sharp signal at 3747 cm^{-1} for $\nu_{(SiOH)}$ (Figure 4b).

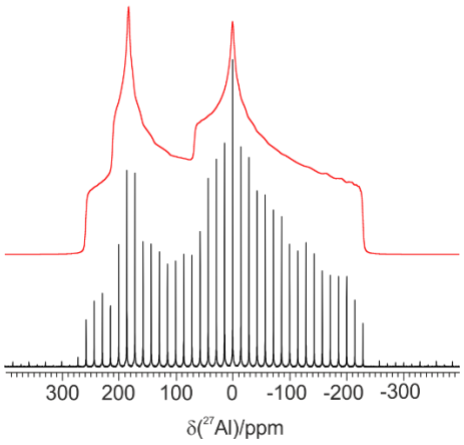

Figure 2. ^{27}Al QCPMG NMR spectrum (208.5 MHz) of **1** along with best-fit simulation (red trace).

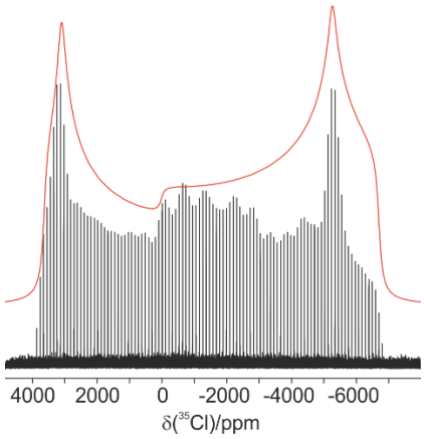

Figure 3. ^{35}Cl WURST-QCPMG NMR spectrum of **1** (78.4 MHz), along with best fit simulation (red trace).

Thus, hybrid material **2** was prepared by reacting complex **1** with Aerosil 380 silica (Evonik, specific area of 380 m^2.g^{-1}) dehydroxylated at 700 °C ($SiO_{2\text{-}700}$, Scheme 2). After stirring for 15 h in pentane at room temperature, repeated washings to remove unreacted **1** and drying under vacuum, **2** was obtained as a white material.

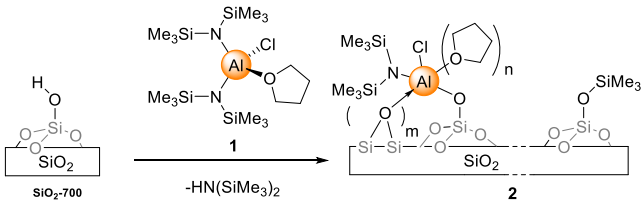

Scheme 2. Synthesis of **2**

Infrared spectra of **1**, $SiO_{2\text{-}700}$ and **2** are compared in Figure 4. The disappearance of the sharp signal at 3747 cm^{-1} within material **2**'s spectrum is in line with a total consumption of non-interacting silanols from $SiO_{2\text{-}700}$, either by reaction with **1** or with HMDS released upon reaction of the Al-N bond with SiO-H.[2] The signals between 3000 and 2795 cm^{-1} are attributed to $\nu_{(sp^3\ C\text{-}H)}$ from $SiMe_3$ and THF groups. No signal accounting for $\nu_{(N\text{-}H)}$ is detected in the 3100-3300 cm^{-1} range.

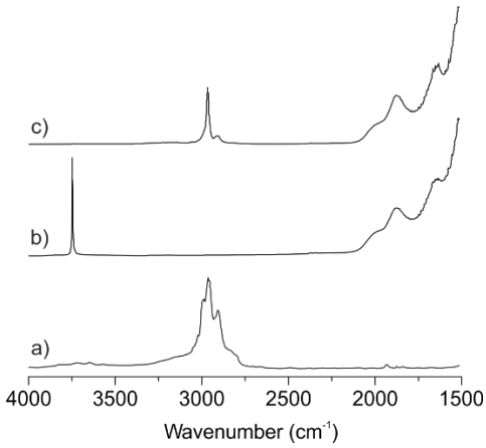

Figure 4. DRIFT of a) **1**, b) $SiO_{2\text{-}700}$ and c) **2**.

Please do not adjust margins

Please do not adjust margins

The aluminium loading within **2** corresponds to an amount of 0.26 mmol.g^{-1}, which is in line with results for the analogous materials prepared from the same silica support and rare-earth amido derivatives[16] (Scheme 2). The N/Al molar ratio is 1.1 as expected from the cleavage of a single aluminium-nitrogen bond by silanolysis as major grafting process (theoretical value: 1.0). NMR tube experiments showed that upon mixing a silica slurry with **1** in C_6D_6, only hexamethyldisilazane?) was detected, no ammonium nor HCl being observed. This rules out the cleavage of Al-Cl by reaction with silanols.

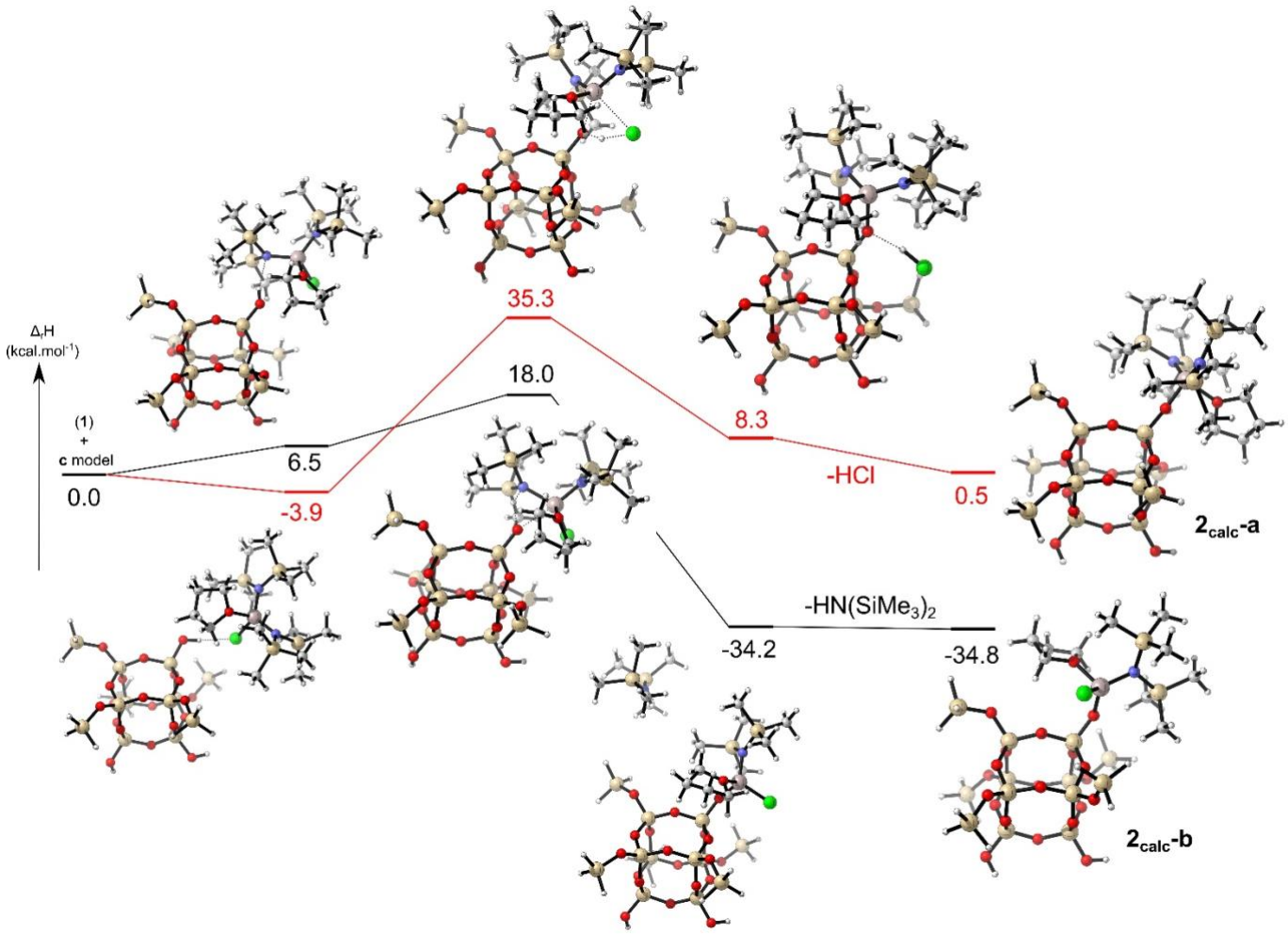

Figure 5. Energy profile for the grafting reaction of **1** onto SiO_{2-700} **c** model. Atoms color scheme: red: O, light pink: Al, green: Cl, grey: C, light brown: Si, white: H, blue: N.

To get better insights on the grafting reaction, the enthalpy profile for the reaction between **1** and SiO_{2-700} was computed at the DFT level (B3PW91). Thus, the grafting reaction has been studied using a polyoligosilsesquioxane derivative as model of the SiO_{2-700} surface (called **c** model). The same strategy has also been successfully used in previous studies[16] to shed light both on the grafting mode of different d/f metal complexes on a silica surface dehydroxylated at 700 °C and on the NMR signature of grafted complexes. Two different reaction pathways have been computed (Figure 5): either *(i)* the Al-N silanolysis with the concomitant $HN(SiMe_3)_2$ production (black pathway in Figure 5) or *(ii)* the Al–Cl silanolysis leading to the release of HCl (red pathway in Figure 5). The grafting reaction begins, in both cases, by the formation of a hydrogen-bonding adduct involving the hydrogen atom of the silanol group of the **c** model and the ligand of interest (either Cl or the silylamide). From an energetic point of view, the formation of the H····Cl adduct (Al–Cl silanolysis pathway) is exothermic with respect to the entrance channel (-3.9 kcal mol^{-1}) whereas the formation of the H····N adduct (Al-N silanolysis pathway) it is endothermic (6.5 kcal mol^{-1}). This stability difference is mainly due to the steric repulsion between the silica surface and **1,** as the formation of the H····N bond implies that **1** comes very close to the silica surface leading to an endothermic adduct. The reaction continues by the grafting of **1** onto the silica surface through either an Al-N silanolysis or an Al–Cl silanolysis. Both reactions are better described as σ-bond metathesis. From a kinetic point of view, the Al-N silanolysis activation barrier (+18.0 kcal mol^{-1}) is lower

This journal is © The Royal Society of Chemistry 20xx

Please do not adjust margins

Please do not adjust margins

than the Al–Cl silanolysis one (+39.2 kcal mol^{-1}). This lowering is due to a better charge distribution at the transition state. As reported by different authors,[17] the charge distribution is of great importance in order to understand the stability of the σ-bond metathesis transition states. In our case, as illustrated in figure 6, the charge of the aluminum, oxygen and hydrogen atoms are similar in both cases. However, the NBO analyses indicates a negative charge of -0,61 for Cl and -1,73 for N. Thus, the negative charge of the nitrogen is strongly stabilized by the presence of the $SiMe_3$ groups leading to a better charge alternation at the transition state and consequently a decrease of the activation barrier. It is also noteworthy that, from a thermodynamic point of view, the formation of **2**$_{calc}$**-b** with the concomitant $HN(SiMe_3)_2$ production is an exothermic process (-34.8 kcal.mol^{-1}) whereas the formation of **2**$_{calc}$**-a** with the concomitant HCl release is an athermic process (+0.5 kcal.mol^{-1}).Thus, in conclusion, the DFT calculations confirm that the major reaction pathway for the reaction of the chloro amide derivative is via protonolysis of the Al-N bond leading to the retention of the Al-Cl moiety upon grafting.

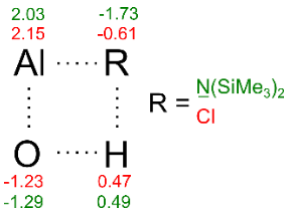

Figure 6. Schematic charge distribution at the transition state of the Al-N silanolysis and Al–Cl silanolysis.

Insights into the molecular-level structure of **2** were obtained thanks to high-field solid-state MAS NMR. The ^{1}H MAS NMR spectrum (Figure 7a) of **2** shows an intense peak at 0.1 ppm with a shoulder at 0.3 ppm, assigned to CH_3 from $SiMe_3$ group of –$N(SiMe_3)_2$ or –$OSiMe_3$. Two weaker signals at 4.2 and 2.0 ppm correspond to α- and β-CH_2 protons from the THF ligand, respectively. The significant shift of the position of α-CH_2 signal in **2** (4.2 ppm) compared to that in **1** (3.65 ppm) indicates coordination of the THF on a more electrophilic metal centre. The ^{13}C CP MAS NMR spectrum of **2** (Supporting Information) features 4 signals. Signals at 2.1 and -1.2 ppm (the former being present as a shoulder) are assigned the methyl groups from either amido ligand or silylated silanols. The presence of the THF ligand is evidenced by the signals at 72 and 24 ppm which account respectively for α and β methylenic carbons. In order to better understand the structure of **2** at the molecular level, a 2D ^{1}H-^{1}H DQSQ MAS NMR spectrum was recorded (Figure 7b). This experiment relies on dipolar interactions between neighbouring protons and thus correlations on this spectrum are related to proximity.[18] First of all, each signal on the 1D spectrum gives rise to self-correlation, as on-diagonal signals, which is expected as these originate from either methyl or methylene groups. Furthermore, three correlations are observed, noted as **A**, **B**, **C** on Figure 7b. Correlation **A**, which associates signals at 4.2 and 2.0 ppm corresponds to the proximity between α– and β–CH_2 protons from THF. Interaction **B**, involving the signal at 4.2 with the signal at 0.1 ppm reveals proximity between α-CH_2 from THF and $AlNSiMe_3$ groups. The same type of interaction is also observed for **C**, which correlates peaks at 2.0 and 0.1 ppm (associating β-CH_2 from THF and $AlNSiMe_3$ protons). The weaker intensity of this latter off-diagonal signal is due to the longer distance between these protons compared to the previous ones. No interaction is detected between $SiMe_3$ groups at 0.3 ppm and THF protons. These can then be assigned to surface aluminium amido centers devoid of coordinated THF ligand or to trimethylsilyl-capped silanols, which are expected to resonate at 0.1 ppm.[19]

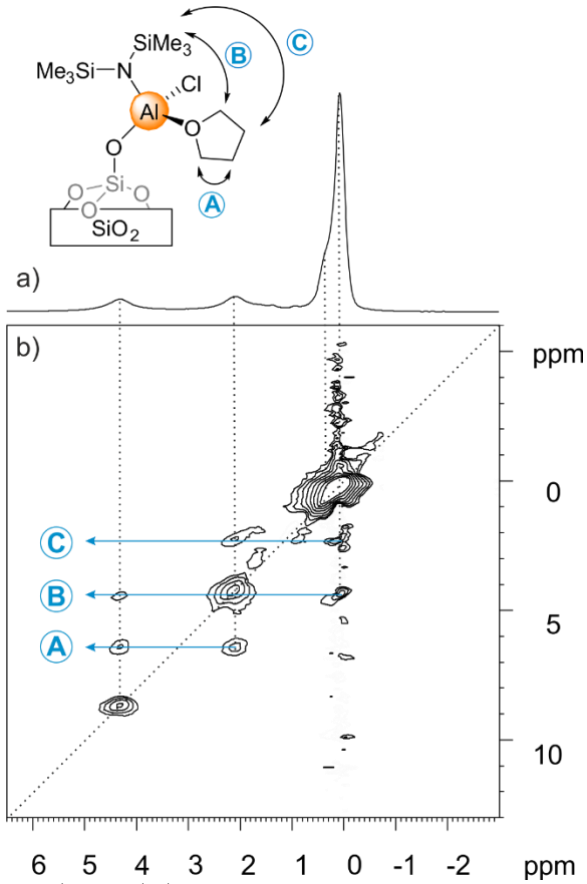

Figure 7. a) ^{1}H and b) ^{1}H-^{1}H DQ-SQ MAS NMR spectra of **2** (18.8 T, spinning speed 20 kHz).

The ^{27}Al echo MAS NMR spectrum of **2** at 18.8 T consists of a broad, complex signal spanning from 95 to 20 ppm, with maxima at about 82 and 65 ppm (Figure 8a). Such chemical shifts correspond to Al nuclei in tetracoordinated configuration. However, this spectrum alone cannot afford meaningful information on the structural feature of supported aluminium species, since quadrupolar parameters cannot be extracted. Indeed, studies on related silica-supported aluminum silylamides showed that their characterization by ^{27}Al MAS NMR was not straightforward.[9] Additional NMR experiments were thus recorded to refine our understanding of material **2**. As a side comment, no ^{35}Cl NMR signal was detected for 2, even with extended recording time. In our own experience, this lack of signal is quite often encountered, due most probably relaxation issues.ref???

Please do not adjust margins

Please do not adjust margins

In first instance, MQ-MAS technique was used to get high resolution ^{27}Al NMR data, and to determine if the signal below 50 ppm stems from chemical shift distribution (and thus, from 5- and 6-coordinated species) or from broadening due to second-order quadrupolar coupling. Indeed, this method provides 2D high-resolution NMR spectra for quadrupolar nuclei, where the indirect dimension presents the isotropic spectrum and the direct one, the second order lineshape. The bidimensional spectrum of **2** is presented on Figure 8f. Two main sites can be distinguished. The first one, corresponding to an isotropic chemical shift of 80 ppm (±5 ppm) features a line shape corresponding to a Czjzeck distributed signal, with a quadrupolar coupling constant of about 7.5 MHz (incertitude, Figure 6c). The second one, of significantly lesser intensity, can be modelled as originated from signal with quadrupolar coupling of about 10.5 MHz (±0.5 MHz), with isotropic chemical shift being distributed between 80 and 70 ppm (Figure 6d). The comparison between the MQ-MAS projection in the anisotropic dimension (Figure 6 b) and the echo MAS NMR spectrum of **2** (Figure 6a) indicates that: 1) the two sites are not as efficiently excited by the MQ-MAS-experiment, with the site featuring the largest C_Q being less responsive; 2) a fraction of the sites (about one fourth of the total signal) below 40 ppm does not give rise to a MQ-MAS signal. These limitations, intrinsic to the MQ-MAS experiment, show the limit of this type of sequence in terms of quantitative information. However, the MQ-MAS data indicates that most of the aluminium centres are tetracoordinated, and they are present as two types of sites, one at higher chemical shift being strongly distributed (as shown by the Czjzeck-distributed lineshape), while the other one, at slightly lower chemical shift, is better defined, with a rather large quadrupolar coupling constant.

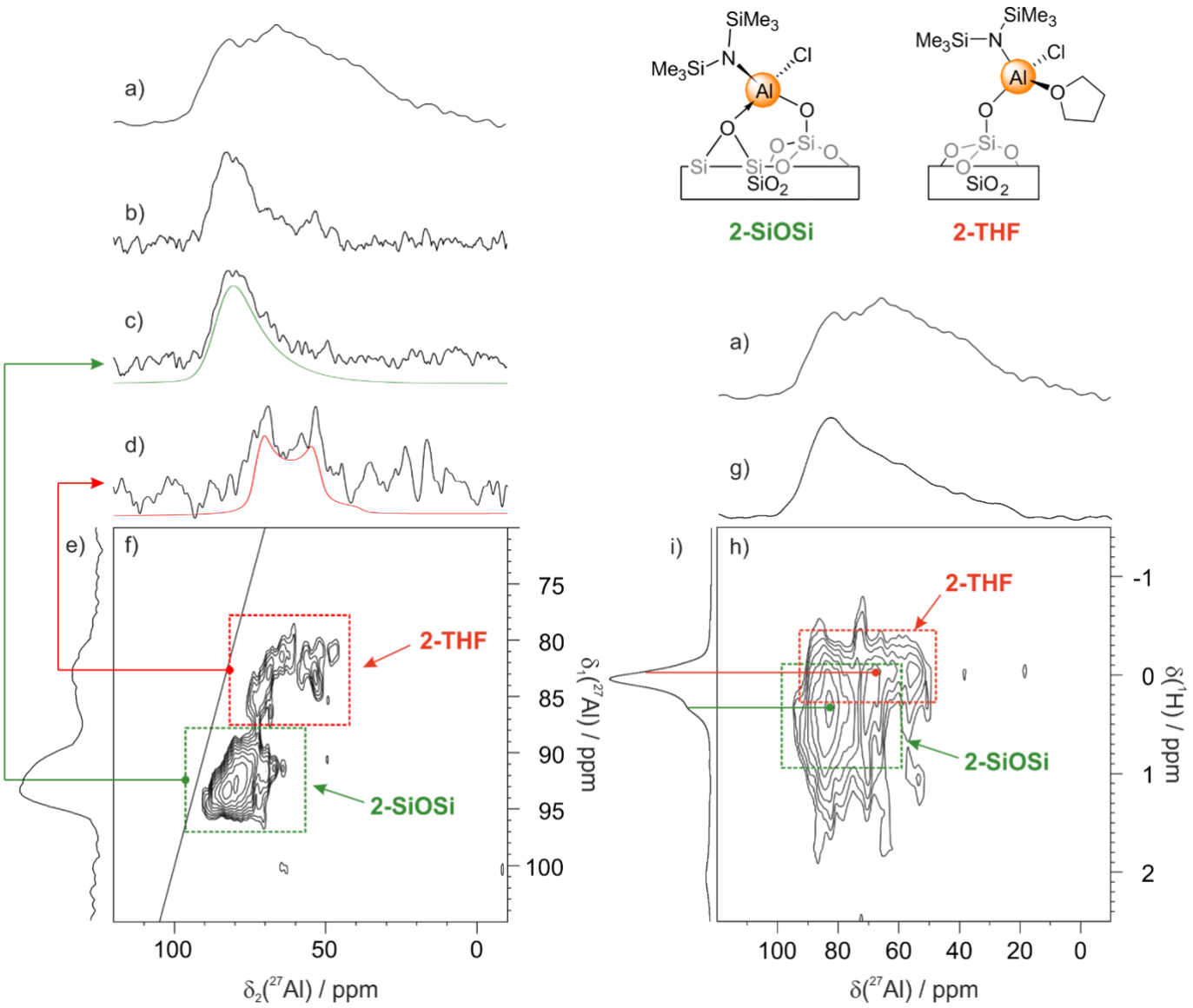

Figure 8. Advanced NMR characterization of **2**: Left part: a) ^{27}Al echo MAS NMR, and MQ-MAS NMR data : b) projection of the anisotropic dimension, c) projection of the 97-87 ppm (isotropic dimension) range in the anisotropic dimension , d) row at 83 ppm (isotropic dimension), e) projection in the isotropic dimension, and f) full MQ-MAS NMR spectrum; Right part: a) ^{27}Al echo MAS and D-HMQC data: g) {^{1}H}-^{27}Al D-HMQC MAS projection, h) ^{1}H-^{27}Al D-HMQC MAS and i) ^{1}H MAS NMR spectra (18.8 T, spinning speed 20 kHz).

This journal is © The Royal Society of Chemistry 20xx

Please do not adjust margins

Please do not adjust margins

Further attempts at gathering detailed structural information on **2** were performed thanks to ^{1}H-^{27}Al D-HMQC NMR, which relies on dipolar interactions between protons and aluminium centres, thus providing information on the heteronuclear proximities within the sample (Right part of Figure 8). On the bidimensional spectrum (Figure 8h), the only interaction observed involves protons at about 0.1 ppm ($SiMe_3$). No clear correlation could be detected between CH_2 protons from the THF ligand and either aluminium site, most probably due to the mobility of the THF ligand. The correlation pattern can be decomposed into two distinct elements: a first pattern linking protons at 0.1 ppm with an aluminium signal from 85 to 50 ppm, and a second pattern involving protons at 0.3 ppm and aluminium centres resonating at 85-60 ppm, with a maximum at 85 ppm. As side comment, the intensity maximum of the former correlation peak is at 0.0 ppm in the ^{1}H dimension, and is slightly shifted compared to the 0.1 ppm maximum observed in the ^{1}H MAS NMR spectrum (Figure 8i). This is consistent with the presence of an overlapping peak from trimethylsilyl-caped silanol ([≡$SiOSiMe_3$]), which do not give rise to ^{1}H-^{27}Al correlations in the D-HMQC spectrum. From the ^{1}H-^{1}H DQSQ MAS NMR spectrum described above (Figure 7b), we know that the protons resonating at 0.1 ppm are close to THF ligands, while the latter are not. These two types of sites have also been separated on the MQ-MAS spectrum described above (Figure 8f). We are thus facing two types of sites, both experiencing isotropic chemical shift distribution, but featuring different quadrupolar couplings. Furthermore, the isotropic chemical shift values of the two sites identified as the major surface species within material **2** are in agreement with aluminium centres in tetracoordinated environment. Thus we propose that these consist of two types of species, designated as **2-SiOSi** and **2-THF**, as depicted on Figure 8. Both species have similar coordination sphere, $AlClNO_2$. However, they differ in the nature of the oxygen-based donor moiety. **2-SiOSi** can be formulated as [(≡SiO)AlCl{$N(SiMe_3)_2$}(≡SiOSi≡)], comprising a siloxane moiety within its coordination sphere. The surface acts here as a L-X type ligand, and the wide structural diversity in terms of bond angles and distances within the silanolate-siloxane framework induces a large distribution within the electrical field gradient for the surface species, which translates into the Czjzeck-type lineshape. On the other hand, part of the grafted species are present as **2-THF**, or [(≡SiO)AlCl{$N(SiMe_3)_2$}(THF)], where a THF ligand is retained within the aluminium coordination sphere. In this case, the structure around the aluminium centre is structurally better defined in terms of bond angles and distances, and is only marginally perturbed by the heterogeneity of the amorphous surface. This translates into the observation of a second order quadrupolar coupling pattern, which broadens the aluminium signal. In order to help further assignment of the experimental data, DFT calculation were performed on a series of potential surface species, built from the aforementioned **c** model and a larger silica model.[20] Figures 9 and 10 present the DFT-optimized structures used to calculate the corresponding NMR parameters listed in Table 1.

Considering the data in Table 1, it appears that the chemical shift is rather dependent from the nature of the coordination sphere. The AlO_2NCl coordination sphere gives rise to chemical shift higher than that of AlO_2N_2 (between 95 and 86 vs. 75 ppm), while the triscoordinate species would feature a higher CS value of about 113 ppm. Comparing the influence of the bound THF *vs.* that of a SiOSi moiety, the chemical shift is overall higher in the latter case (94.3-87.2 ppm range compared to 85.0-85.7 ppm), in line with the proposed assignment for the two sites.

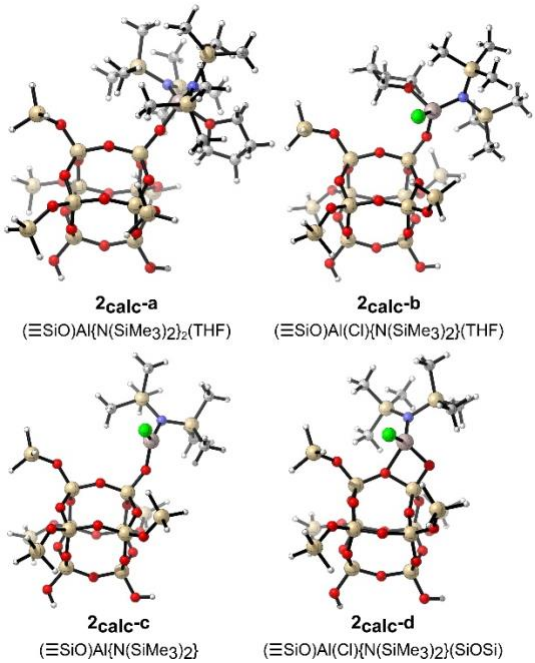

Figure 9. DFT-optimized models for the surface species **2** built from the **c** model.

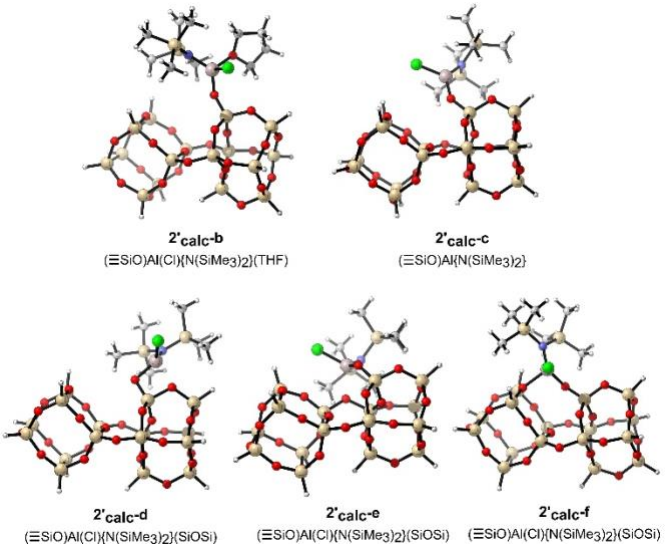

Figure 10. DFT-optimized models for the surface species **2** built from a larger silica surface model.

Please do not adjust margins

Please do not adjust margins

When considering the quadrupolar coupling constants, the species featuring bound THF give rise to lower values compared to those of the siloxane adducts (16.5-18.9 MHz for the **2**$_{calc}$-**b** and **2'**$_{calc}$-**b** configurations *vs.* 20.7-25.9 MHz for the **2**$_{calc}$-**d**, **2'**$_{calc}$-**d**, **2'**$_{calc}$-**e** and **2'**$_{calc}$-**f** configurations). These are all above the experimentally deduced 7.5 and 10.5 MHz values. Such discrepancy may result from several factors. One has been mentioned above, which is the difficulty in efficiently recording the expected broad signals with MQ-MAS. Another cause can be linked to the limits of the models used for calculations, as shown in the case of [(≡SiO)AlCl{N(SiMe$_3$)$_2$}(≡SiOSi≡)]: The quadrupolar coupling constant values are within a 5.2 MHz window (about 25% of the considered C_Q values), which gives an indication of the expected distribution. On the other hand, the combination of both chemical shift and quadrupolar coupling constant could give rise to a line shape from unambiguous extraction of NMR parameters is not possible under the present technical and experimental conditions [Laurent]. Regarding the triscoordinated species, **2**$_{calc}$-**c** and **2'**$_{calc}$-**c** give rise to a value of *ca.* 37 MHz, as expected from the large electrical field gradient resulting from the trigonal planar configuration.[11] Such values are not to be taken as such (as these C_Q values would result in non-observable signals), but should rather be used to estimate trends from which conclusions could be drawn to better understand our experimental results on the supported species. As a further comment on these discrepancies and technical limitations, the difficulty in recording and extracting NMR parameters from solid state NMR of the grafted metal itself was also experienced in the case of the surface chemistry of the related [Sc{N(SiMe$_3$)$_3$}] species.[21] Indeed, whereas molecular precursors afford ^{45}Sc NMR lineshape characteristic of strong quadrupolar coupling, the material resulting from their grafting does only give rise to broad, featureless signals, from which straightforward assessment of NMR parameters is out of reach.

Experimental

General Considerations.

Manipulations were carried out under argon atmosphere in an M-Braun glove-box or by using Schlenk techniques. THF and pentane were dried by using conventional reagents and stored in the glove-box over 3Å molecular sieves. Liquid-state NMR spectroscopic analyses were run with a Bruker Avance 300 spectrometer. Solid-state MAS NMR spectra were recorded on a Bruker Avance 800 spectrometer (^{1}H: 800.13 MHz, ^{27}Al: 208.49 MHz, ^{35}Cl: XXX MHz). For ^{1}H experiments, the spinning frequency was 20 kHz, the recycle delay was 10 s and 16 scans were collected with a 90° pulse excitation of 3.5 µs. The two-dimensional homonuclear experiment (DQ-MAS) was obtained at a spinning frequency of 20 kHz by using excitation and reconversion pulse blocks of two rotor periods each (200 µs). The 90° pulse length was 2.25 µs, the recycle delay was 10 s, and 32 scans were collected for each slice (256 in total). The ^{1}H-^{27}Al HMQC experiment were set up with a ^{27}Al spin echo selective to the central transition, with pulses of x and x µs, with ^{1}H π/2 pulse of 3.5 µs on either side of the ^{27}Al π pulse. The number of scans for each t_1 increment was set to 4090. The ^{27}Al MAS spectra at 18.8T were acquired at a spinning frequency of 20 kHz. The MQMAS spectra were collected using the Z-filter sequence, which consists of two hard pulses of 3.5 and 1.3 µs at an RF field of 90 kHz, for triple-quantum excitation and reconversion, respectively, followed by a soft pulse of 6 µs at an RF field of 15 kHz (check). The t_1 step was set to the MAS period. Chemical shifts were given in ppm with respect to TMS as external reference for ^{1}H NMR, and to Al(H$_2$O)$_6^{3+}$ for ^{27}Al NMR. Diffuse reflectance infrared spectra were collected with a Harrick cell on a Nicolet 6700 FT-IR spectrometer fitted with a MCT detector. Elemental analyses were conducted at London Metropolitan University (CHN) and at LASIR, University of Lille (Al).

Synthesis of 1 : Li[N(SiMe$_3$)$_2$](THF) (5 g, 21.0 mmol, 2 eq) was added to freshly sublimed AlCl$_3$ (1.4 g, 10.5 mmol) in toluene (30 mL) and the reaction mixture was stirred for 3 days at room temperature. Volatiles were removed by heating the mixture under vacuum for 3 hours at 100 °C. After extraction with pentane and crystallization at -40 °C, white crystals are obtained (3.80 g, 80 % yield). ^{1}H NMR (300 MHz, C$_6$D$_6$): δ 4.0 (4H, t, OCH$_2$), 1.1 (4H, t, OCH$_2$CH$_2$), 0.4 (36H, s, SiMe$_3$). ^{13}C NMR (75.5 MHz, C$_6$D$_6$): δ 74.0 (α–CH$_2$ from THF), 24.8 (β–CH$_2$ from THF), 6.2 (SiMe$_3$). Elemental analysis: C, 41.97; H, 9.61; N, 5.92. Theor: C, 42.21; H, 9.74; N, 6.15

Synthesis of 2: A double-Schlenk vessel was loaded with a 10 mL pentane solution of **1** (160 mg, 0.35 mmol) in one compartment and with silica dehydroxylated at 700 °C (1 g) with 10 mL of pentane in the other compartment. After 15 h of stirring, the supernatant liquid was then separated by filtration into the other compartment, from which the solvent was gas-phase transferred by trap-to-trap distillation back into the compartment containing the modified support in order to wash away any residual molecular precursor or adsorbed compounds. This operation was repeated thrice and resulting material **2** was dried under secondary vacuum (10^{-6} mbar) at room temperature for 14 h. Elemental analysis: C, 3.34; H, 0.71; N, 0.41; Al 0.71.

Computational details. All DFT calculations were performed with Gaussian 09.[22] Geometries were fully optimized in gas phase without symmetry constraints, employing the B3PW91 functional[23] and the Stuttgart effective core potential for Al and Si [24] augmented with a polarization function (ζ_d = 0,284 for Si and ζ_d = 0.325 for Al). For the other elements (Cl, N, H, C and O), Pople's double-ζ basis set 6-31G(d,p)[25] was used. Calculations of vibrational frequencies were systematically done in order to characterize the nature of stationary points. Calculating a theoretical chemical shift requires the knowledge of the chemical shielding of a reference, since it is explicitly calculated as $\delta_{iso} = (\sigma_{iso,ref} - \sigma_{iso,sample})$, in ppm. The ^{27}Al and ^{35}Cl chemical shift values of **1** were used to calibrate the theoretical $\sigma_{iso,ref}$.values (namely, the experimental value was selected as reference for ^{27}Al and ^{35}Cl chemical shift calibrations). As a consequence, for ^{35}Cl, the calculated $\sigma_{iso,sample}$ of 928,25 ppm is attributed to an experimental CS of 90 ppm: $\sigma_{iso,ref}$ (Cl) = 1018,25 ppm. For ^{27}Al, the calculated $\sigma_{iso,sample}$ of 469,52 ppm is attributed to

This journal is © The Royal Society of Chemistry 20xx

Please do not adjust margins

Please do not adjust margins

an experimental CS of 95 ppm: $\sigma_{iso,ref}$ (Al) = 564,52 ppm. Among the various theories available to compute chemical shielding tensors, the gauge including atomic orbital (GIAO) method has been adopted for the numerous advantages it presents.[26] The same methodology was used in previous studies involving grafted systems, showing that theoretical results are fairly accurate with respect to experimental values with an error lower than 15% for ^{29}Si,[27] 10% for ^{31}P [28] and ^{17}O [4,16] and 5% for ^{1}H [29] and ^{13}C[29]. The quadrupolar coupling constant C_Q and the asymmetry parameter η_Q, which describes the interaction between the nuclear quadrupolar moment of the oxygen nuclei and the electric field gradient (EFG) arising at these sites, are calculated from the EFG tensor eigenvalues V_{11}, V_{22}, and V_{33} with the convention: $|V_{33}| \geq |V_{22}| \geq |V_{11}|$.

$$C_Q = (eQV_{33}) / h \qquad (1)$$

The conversion from atomic units to MHz is given in Equation (2).

$$C_Q = -2{,}3496.Q.V_{33} \qquad (2)$$

In this work an effective Q value of -14,66 fm^2 has been used for ^{27}Al and -8,165 fm^2 for ^{35}Cl. The electron density and partial charge distribution were examined in terms of localized electron-pair bonding units using the NBO program[30] available in Gaussian 09.

Conclusions

A new heteroleptic bis-amidochloro aluminum species was prepared and structurally characterized. Its grafting on dehydroxylated silica led to the formation of two main types of species, both featuring tetracoordinated coordination sphere, and differing in the nature of the oxygen-based donor ligand (THF or siloxane). These structural elements were determined thanks to mostly ^{27}Al MAS NMR, combined with DFT calculations. This study thus shows how high-field solid-state NMR can bring a deeper insight into the structure of grafted species, especially when combined with DFT calculations. However, it also illustrates how challenging such deceivingly simple systems can be, when aiming at their full understanding at the molecular level.

Conflicts of interest

There are no conflicts to declare.

Acknowledgements

Chevreul Institute (FR 2638), Ministère de l'Enseignement Supérieur et de la Recherche, CNRS, Région Nord – Pas de Calais and FEDER are acknowledged for supporting and funding partially this work. The authors acknowledge the HPCs CALcul en Midi-Pyrénées (CALMIP-EOS grant 0833).

Notes and references

1 M. Lappert, A. Protchenko, P. Power and A. Seeber, *Metal Amide Chemistry*, 2009, Wiley-VCH (Weinheim)
2 Y. Liang and R. Anwander, *Dalton Trans.*, **2013**, *42*, 12521.
3 C. Copéret, A. Comas-Vives, M. P. Conley, D. P. Estes, A. Fedorov, V. Mougel, H. Nagae, F. Núñez-Zarur and P. A. Zhizhko, *Chem. Rev.*, **2016**, *116*, 323; M. K. Samantaray, E. Pump, A. Bendjeriou-Sedjerari, V. D'Elia, J. D. A. Pelletier, M. Guidotti, R. Psaro and J.-M. Basset, *Chem. Soc. Rev.* **2018**, *47*, 8403.
4 D. Grekov, T. Vancompernolle, M. Taoufik, L. Delevoye and R. M. Gauvin, *Chem. Soc. Rev.*, **2018**, *47*, 2572.
5 N. Merle, J. Trébosc, A. Baudouin, I. Del Rosal, L. Maron, K. Szeto, M. Genelot, A. Mortreux, M. Taoufik, L. Delevoye and R. M. Gauvin, *J. Am. Chem. Soc.* **2012**, *134*, 9263; Y. Bouhoute, D. Grekov, N. Merle, K. C. Szeto, A. De Mallmann, F. Lefebvre, G. Raffa, I. Del Rosal, L. Maron, R. M. Gauvin, L. Delevoye and M. Taoufik, *ACS Catal.*, **2016**, *6*, 1.
6 J. Pump, E. G. Rochow and U. Wannagat, *Angew. Chem. Internat. Ed.*, **1963**, *2*, 264; G. M. Sheldrick and W. S. Sheldrick, *J. Chem. Soc. A*, **1969**, 2279-2282.
7 M. P. Coles, *Coord. Chem. Rev.*, **2015**, *24–39*, 297-298.
8 K. J. L. Paciorek, J. H. Nakahara and S. R. Masuda, *Inorg. Chem.* **1990**, *29*, 4252-4255; M. Garcia-Castro, A. Martin, M. Mena and C. Yélamos, *Chem. Eur. J.* **2009**, *15*, 7180 – 7191.
9 R. Anwander, C. Palm, G. Gerstberger, O. Groeger and G. Engelhardt, *Chem. Commun.*, **1998**, 1811 ; G. Gerstberger, C. Palm and R. Anwander, *Chem. Eur. J.* **1999**, *5*, 997.
10 K. R. D. Johnson and P. G. Hayes, *Polyhedron*, **2016**, *108*, 43.
11 J. A. Tang, J. D. Masuda, T. J. Boyle and R. W. Schurko, *ChemPhysChem*, **2006**, *7*, 117.
12 R. W. Schurko, *Acc. Chem. Res.* **2013**, *46*, 1985.
13 A. J. Rossini, R. W. Mills, G. A. Briscoe, E. L. Norton, S. J. Geier, I. Hung, S. Zheng, J. Autschbach and R. W. Schurko, *J. Am. Chem. Soc.* **2009**, *131*, 3317; K. E. Johnston, C. A. O'Keefe, R. M. Gauvin, J. Trébosc, L. Delevoye, J.-P. Amoureux, N. Popoff, M. Taoufik, K. Oudatchin and R. W. Schurko, *Chem. Eur. J.* **2013**, *19*, 12396; C. A. O'Keefe, K. E. Johnston, K. Sutter, J. Autschbach, R. M. Gauvin, J. Trébosc, L. Delevoye, N. Popoff, M. Taoufik, K. Oudatchin and R. W. Schurko, *Inorg. Chem.* **2014**, *53*, 9581.
14 R. Anwander and P.W. Roesky, *J. Chem. Soc. Dalton Trans.*, **1997**, 137.
15 R. M. Gauvin and A. Mortreux, *Chem. Commun.* **2005**, 1146; R. M. Gauvin, L. Delevoye, R. Ali Hassan, J. Keldenich and A. Mortreux, *Inorg. Chem.* **2007**, *46*, 1062.
16 I. del Rosal, I. C. Gerber, R. Poteau and L. Maron, *J. Phys. Chem. A*, **2010**, *114*, 6322; N. Merle, G. Girard, N. Popoff, A. De Mallmann, Y. Bouhoute, J. Trébosc, E. Berrier, J.-F. Paul, C. P. Nicholas, I. Del Rosal, L. Maron, R. M. Gauvin, L. Delevoye and M. Taoufik, *Inorg. Chem.*, **2013**, *52*, 10119; Y. Bouhoute, A. Garron, D. Grekov, N. Merle, K. C. Szeto, A. De Mallmann, I. Del Rosal, L. Maron, G. Girard, R. M. Gauvin, L. Delevoye and M. Taoufik, *ACS Catal.*, **2014**, *4*, 4232; I. del Rosal, I. C. Gerber, R. Poteau and L. Maron, *New J. Chem.*, **2015**, *39*, 7703; Y. Bouhoute, I. Del Rosal, K. C. Szeto, N. Merle, D. Grekov, A. De Mallmann, E. Le Roux, L. Delevoye, R. M. Gauvin, L. Maron and M. Taoufik, *Catal. Sci. Technol.*, **2016**, *6*, 8532; T. Vancompernolle, A. Valente, T. Chenal, P. Zinck, I. Del Rosal, L. Maron, M. Taoufik, S. Harder and R. M. Gauvin, *Organometallics*, **2017**, *36*, 3912–3920
17 L. Werkema, E. Messines, L. Perrin, L. Maron, O. Eisenstein and R. A. Andersen, *J. Am. Chem. Soc.,* **2005**, *127*, 7781 ; R. Waterman, *Organometallics*, **2013**, *32*, 7249; L. Castro, A. Yahia, L. Maron, *Dalton Trans.*, **2010**, *39*, 6682.
18 I. Schnell, S. P. Brown, H. Y. Low, H. Ishida and H. W. Spiess, *J. Am. Chem. Soc.*, **1998**, *120*, 11784.
19 R. Anwander, I. Nagl and M. Widenmeyer, *J. Phys. Chem. B*, **2000**, *104*, 3532.
20 B. Werghi, A. Bendjeriou-Sedjerari, J. Sofack-Kreutzer, A. Jedidi, E. Abou-Hamad, L. Cavallo and J.-M. Basset, *Chem. Sci.* **2015**, *6*, 5456.

Please do not adjust margins

Please do not adjust margins

21 T. Vancompernolle, X. Trivelli, L. Delevoye, F. Pourpoint and R. M. Gauvin, *Dalton Trans.* **2017**, *46*, 13176.

22 Gaussian 09, Revision D.01, M. J. Frisch, G. W. Trucks, H. B. Schlegel, G. E. Scuseria, M. A. Robb, J. R. Cheeseman, G. Scalmani, V. Barone, G. A. Petersson, H. Nakatsuji, X. Li, M. Caricato, A. Marenich, J. Bloino, B. G. Janesko, R. Gomperts, B. Mennucci, H. P. Hratchian, J. V. Ortiz, A. F. Izmaylov, J. L. Sonnenberg, D. Williams-Young, F. Ding, F. Lipparini, F. Egidi, J. Goings, B. Peng, A. Petrone, T. Henderson, D. Ranasinghe, V. G. Zakrzewski, J. Gao, N. Rega, G. Zheng, W. Liang, M. Hada, M. Ehara, K. Toyota, R. Fukuda, J. Hasegawa, M. Ishida, T. Nakajima, Y. Honda, O. Kitao, H. Nakai, T. Vreven, K. Throssell, J. A. Montgomery, Jr., J. E. Peralta, F. Ogliaro, M. Bearpark, J. J. Heyd, E. Brothers, K. N. Kudin, V. N. Staroverov, T. Keith, R. Kobayashi, J. Normand, K. Raghavachari, A. Rendell, J. C. Burant, S. S. Iyengar, J. Tomasi, M. Cossi, J. M. Millam, M. Klene, C. Adamo, R. Cammi, J. W. Ochterski, R. L. Martin, K. Morokuma, O. Farkas, J. B. Foresman and D. J. Fox, Gaussian, Inc., Wallingford CT, **2016**.

23 A. D. Becke, *J. Chem. Phys.* **1993**, *98*, 5648 and references therein ; (b) K. Burke, J. P. Perdew and W. Yang, Electronic Density Functional Theory: Recent Progress and New Directions; Plenum: New York, **1998**.

24 A. Bergner, M. Dolg, W. Kuechle, H. Stoll and H. Preuss, *Mol. Phys.*, **1993**, *80*, 1431.

25 P. C. Hariharan and J. A. Pople, *Theor. Chem. Acc.*, **1973**, *28*, 213. (b) W. J. Hehre, R. Ditchfield and J. A. Pople, *J. Chem. Phys.* **1972**, *56*, 2257.

26 F. J. London, *J. Phys. Radium*, **1937**, *8*, 397; R. McWeeny, *Phys. Rev.*, **1962**, *126*, 1028; R. Ditchfield, *Mol. Phys.*, **1974**, *27*, 789; J. L. Dodds, R. McWeeny and A. J. Sadlej, *Mol. Phys.*, **1977**, *34*, 1779.

27 I. del Rosal, I. C. Gerber, R. Poteau and L. Maron, *J. Phys. Chem. A*, **2010**, *114*, 6322.

28 H. Staub, I. Del Rosal, L. Maron, F. Kleitz and F.-G. Fontaine, *J. Phys. Chem. C*, **2012**, 116, 25919

29 N. Popoff, J. Espinas, J. Pelletier, B. Macqueron, K. C. Szeto, O. Boyron, C. Boisson, I. Del Rosal, L. Maron, A. De Mallmann, R. M. Gauvin and M. Taoufik, *Chem. Eur. J.*, **2013**, *19*, 964.

30 A. E. Reed, L. A. Curtiss and F. Weinhold, *Chem. Rev.* **1988**, *88*, 899.

This journal is © The Royal Society of Chemistry 20xx

Please do not adjust margins